

Binomial Line Cox Processes: Statistical Characterization and Applications in Wireless Network Analysis

Mohammad Taha Shah, *Graduate Student Member, IEEE*, Gourab Ghatak, *Member, IEEE*, Souradip Sanyal, and Martin Haenggi, *Fellow, IEEE*

Abstract—The current analysis of wireless networks with transceivers confined to streets is primarily based on Poissonian models, such as Poisson line processes and Poisson line Cox processes. We demonstrate important scenarios where a model with a finite and deterministic number of streets, termed the binomial line process (BLP), is more accurate. We characterize the statistical properties of the BLP and the corresponding binomial line Cox process (BLCP) and apply them to analyze the performance of a network whose access points are deployed along the streets of a city. Such a deployment scenario will be typical for 5G and future wireless networks. In order to obtain a fine-grained insight into the network performance, we derive the meta distribution of the signal-to-interference and noise ratio. Accordingly, we investigate the mean local delay in transmissions and the density of successful transmission. These metrics, respectively, characterize the latency and coverage performance of the network and are key performance indicators of next-generation wireless systems.

Index Terms—Stochastic geometry, Line processes, Cox process, Wireless communications

I. INTRODUCTION

A. Motivation

Line processes are useful statistical tools for studying various engineering problems such as transportation and urban infrastructure planning, wireless communications, and industrial automation scenarios [3], [4]. In the two-dimensional Euclidean plane, a line process is a random collection of lines whose locations and orientations reside in a parameter space (to be defined shortly) according to a spatial stochastic process. Leveraging a line process, researchers often study doubly stochastic processes called Cox processes, which are Poisson point processes defined with the line process as their restricting domain [5]. These models are key in deriving insights into engineering and planning questions such as: 1) *How many electric vehicle charging points does a city need to have along the streets?* 2) *From a typical urban home, how far is the*

nearest bus stop? Accordingly, what should be the density of bus stops in a given city? 3) *For on-road deployments of wireless small cells as envisaged in 5G and future networks, what would be the cellular coverage performance of a user in the city?* In the context of wireless communications in particular, AT&T plans to deploy compact Ericsson street radio small cells integrated with the street lights to accelerate 5G deployments [6]. Similarly, New York City has already deployed such small cells focusing on high-speed connectivity for pedestrian users [7]. Such deployments seamlessly integrate access points (APs) in the urban infrastructure to provide ubiquitous connectivity to the users. In this regard, the network coverage of any point in the network for such on-street deployed small cells is a significant point of interest for network operators.

In this paper, we examine a novel line process called BLP, which is a shift from the traditional Poisson processes used in wireless communication. Our research has shed light on the key characteristics of the BLP and the Cox process driven by it, i.e., the binomial line Cox process (BLCP), providing new insights into how they can be applied to wireless communication scenarios in practical urban settings. The BLP and BLCP offer a more accurate depiction of road networks in both urban and suburban areas, taking into account varying levels of density and street structures. By analyzing the density characteristic of BLP, it can be used for optimizing the placement of APs, reconfigurable intelligent surfaces (RIS) deployment, vehicle charging points, and estimating accident-prone intersection areas, among others.

B. Related Work

In the literature, several line processes have been used to study the structure of streets, e.g., the PLP, the Poisson Voronoi tessellation (PVT), and the Poisson lilypond model [9]–[15]. Of all the candidate line processes, the most popular one for modeling streets, especially in wireless network studies, is the PLP. The doubly stochastic Poisson process driven by the PLP was first studied in [9] where the author has characterized the Palm distribution and the Laplace functional of the Poisson line Cox process (PLCP) and employed it to study the coverage performance of a wireless network. The statistical properties of the PLP provide significant tractability in developing insights into the engineering problems of interest. For example, in [16], the authors have employed the PLCP for

Mohammad Taha Shah is with the Bharti School of Telecommunication Technology and Management, IIT Delhi (email: bsz218183@iitd.ac.in). Gourab Ghatak is with the Department of Electrical Engineering, IIT Delhi, India (email: gghatak@ee.iitd.ac.in). Souradip Sanyal is with Continental AG. He was with the Department of Electronics and Communication Engineering IIIT-Delhi at the time of this work (email: souradip20156@iiitd.ac.in). Martin Haenggi is with the Department of Electrical Engineering, University of Notre Dame, Notre Dame, IN 46556 USA (e-mail: mhaenggi@nd.edu).

The codes for generating the numerical results of this paper are available for download [1]. A part of this work was presented in the Workshop on Spatial Stochastic Models for Wireless Networks (SpaSWiN), 2023 [2].

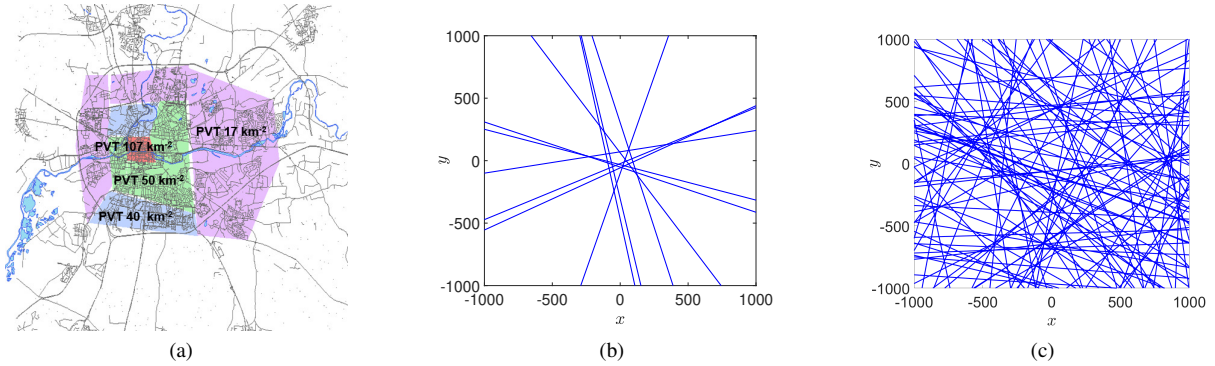


Fig. 1. PVT models for fitting for streets of Lyon [8]. For a PVT, the model parameter is the underlying Poisson point process (PPP) density, (b) A BLP with $n_B = 10$ and $R = 100$ (c) A Poisson line process (PLP) whose underlying PPP has intensity $\frac{n_B}{2\pi R}$ with $n_B = 10$ and $R = 100$. Note: Here, R is the circle's radius in which BLP lines are generated.

	PLP	BLP
Generating domain	Open Cylinder: $\mathcal{D} := [0, \pi) \times (-\infty, \infty)$	Closed Cylinder: $\mathcal{D} := [0, \pi) \times [-R, R]$
Intensity of point process	λ	-
Number of points	Poisson Distributed - $\frac{(2\pi\lambda R)^k e^{-(2\pi\lambda R)}}{k!}$	Fixed - n_B
Dist. of points in \mathcal{D}	$\theta \sim \mathcal{U}[0, \pi], r \sim \mathcal{U}[-R, R]$	$\theta \sim \mathcal{U}[0, \pi], r \sim \mathcal{U}[-R, R]$
Spatial Distribution	Homogeneous	Non-homogeneous

Table I: Difference between PLP and BLP.

studying the on-street deployment of small cell base stations (BSs) and derived the performance of a pedestrian user in a multi-tier multi radio access technique (RAT) cellular network. Choi *et al.* [17] introduce an integrated design for cellular networks, in which the BSs are distributed according to a PPP, and vehicles act as both BSs and users. It simulates the distribution of vehicles using PLCP, and uses Palm calculus to analyze statistical aspects like coverage probability and user association. The authors then extended their work in [18], [19], and [20] where they first analyze statistical properties of the PLCP to an extensive scale, then model and analyze the performs of a vehicular network in correlated blockages; eventually they develop a framework to analyze user behavior in a PLCP-based vehicular network with road-side units (RSUs) and vehicle relays, thus determining user behavior changes in a heterogeneous network. Furthermore, Choi *et. al* in [21], have developed an analytical framework to examine the line-of-sight (LOS) coverage area in vehicular networks.

Chetlur *et. al* in [22] have studied a vehicular network with wireless nodes distributed along roads using Poisson processes to model roadways and node locations, determining coverage probability for a typical receiver while addressing interference challenges. Similarly, in [23], [24], the authors have characterized the performance of C-V2X networks based on the PLP model for streets and, consequently, PLCP for emulating vehicular nodes. Recently, authors in [25] explore the analytical characterization of the Manhattan Poisson line Cox process (MPLCP) but are yet to provide a vehicular network framework for performance analysis. Likewise, authors in [26] explore a stochastic framework for the application of platooning using a triply-stochastic point process PLP-MCP and derive load distribution served by the typical BS. However, one major drawback of the PLP is that it fails to accurately consider some salient features of urban street networks, e.g., finite street lengths, T-junctions, and varying density of streets

across a given city. In [27], authors have introduced a trans-dimensional approach to simplify the analysis of complex vehicular network models, proving improved accuracy under shadowing offering insights for network congestion control even for non-linear street geometries. The recent work by Jeyaraj *et al.* [12] proposed a generalized framework for Cox models to study vehicular networks. The authors significantly improved the accuracy of line process models to account for finite street lengths by considering T-junctions, stick processes, and Poisson lilypond models. However, their work does not consider varying line densities from the perspective of a single city. This is an important aspect of applications such as urban transport networks and wireless deployment planning, in which streets near the city center are denser than in the suburbs. This paper primarily examines the characteristics of these urban scenarios using a non-homogeneous line process.

To illustrate this, in [8], researchers have emulated the streets of Lyon with multi-density Poisson-Voronoi tessellations (PVTs) and Poisson line tessellations (PLTs). Details on the mathematical framework to develop these models can be found in [28]. As shown in Fig. 1a, the authors tuned the parameters of the PVT model to emulate the distinct street structures in different parts of the city, e.g., the red-colored zone corresponds to a PPP of intensity 107 km^{-2} as compared to the green (PPP with intensity 50 km^{-2}) or purple. In contrast, this paper introduces a novel stochastic line process that, with a fixed set of parameters, can emulate distinct street layouts in both the city center and suburbs.

Furthermore, since the city administrations construct the streets on a case-by-case basis, a deterministic number of streets is more likely to characterize the street network in a city. In essence, for initial infrastructure planning, it's more relevant to address the questions mentioned when a specific number of streets, denoted as n_B , exists in a city rather than focusing on street density. This prompts us to study the

Features	Our work	[29]	[17]	[22] [5]	[27]
Decreasing lines	✓	✓	✗	✗	✗
Spatial characterization of line process	✓	✗	✗	✓	✓
Non-homogeneous density of AP/BS	✓	✗	✗	✗	✗
Success probability	✓	✗	✓	✓	✓
Performance analysis w.r.t. location of user	✓	✗	✗	✗	✗
Meta distribution	✓	✗	✗	✗	✓
Network optimization	✓	✗	✗	✗	✓

Table II: Difference between our work and other papers.

properties of the street network parameterized by n_B .

To address these aspects of urban street networks, recently, in a short note, we have introduced the BLP as a new stochastic line process that consists of a deterministic number of lines generated in a bounded generating set [29]. Fig. 1 shows a realization of BLP and PLP, which helps us visualize the difference in the network formed by them. In Fig. 1b, we plot a BLP realization with $n_B = 10$ streets within a distance of $R = 100$ from the origin, contrasting it with a PLP realization in Fig. 1c where the generating PPP has an intensity of $n_B/(2\pi R) = 0.016$. It is apparent that the BLP captures a single city's varying street length densities by virtue of its non-stationarity, while the stationary PLP-based models are limited to a single fixed density. Table I points out the major difference between BLP and PLP. As will be revealed later, the BLP is either characterized by its model parameters - n_B and R (the city radius), or its statistical features such as the line length density and the intersection density.

Difference from the existing works: Table II effectively highlights the differences between existing works and this paper. In contrast to the existing literature, this paper offers a fresh perspective on the non-homogeneous spatial geometry of road structures in urban and sub-urban cities. None of the existing papers have considered such a stochastic model and developed a framework for location-based performance analysis of users in a city. Ghatak in [29] introduced the novel BLCP model and derived its distance-based probability distributions. However, the work [29] is just an introduction, and it does not truly characterize the BLP as a prospective model for modeling road networks. Likewise, in comparison to papers mentioned in Table II, our work showcases its novelty. Most of the features of our work are absent from other papers. While some characteristics may be ubiquitous, they are not truly common due to the complexity of the non-homogeneous line process model.

C. Contributions

This research presents a novel viewpoint on the non-uniform spatial configuration of road networks in urban and suburban areas, which differs from the overly simplistic PLCP and other homogeneous Cox vehicular network models. The statistical characterization of the model validates its non-homogeneous nature and how closely it resembles real-world road networks. We present an analytical method for determining network performance based on a user's location in a city. The following

sections provide technical details on spatial characteristics and system-level insights.

1) *Characterization of BLP:* First, we characterize the statistical properties of the BLP, where we derive the radial density features - the line length density and the intersection density for the BLP. By comprehensively analyzing these properties, we better understand BLP dynamics and show its resemblance to real-world road networks. Furthermore, we derive the distance distribution to the nearest intersection point of a BLP from a given test point. Although critical in analyzing real-world networks, these aspects of a BLP have not been previously reported in the literature.

2) *Derivation of Probability Generating Functional:* Then, we derive the probability generating functional (PGFL) of a shifted and reduced version of BLCP. Importantly, BLCP requires careful treatment and analysis due to its reduced palm distribution compared with traditional PLCP due to the fixed number of lines in the former.

3) *Transmission Success Probability:* Leveraging the obtained PGFL, we analyze the transmission success probabilities in wireless networks with APs locations modeled by a BLCP. We assume that the receiver is connected to its nearest transmitting node in the network. This model is adaptable for simulating various network scenarios, such as Wi-Fi, APs in industrial environments, on-street 5G small cell deployments, etc. Unlike standard stationary models like PPP and PLCP, which are limited to uniform setups, our analysis shows insights into the location-based performance of a user.

4) *Meta Distribution of SINR:* We delve deeper into the analysis of wireless networks modeled using the BLCP by characterizing the meta distribution of the signal-to-interference-plus-noise ratio (SINR). Specifically, we derive the moments of the conditional success probability to study the mean local delay and the density of successful transmissions, providing valuable insights into network latency and coverage. Subsequently, we analyze the optimum transmission probability in the ALOHA scheme, which minimizes the delay depending on the location of the user.

D. Notations

Line processes are denoted by calligraphic letters, e.g., \mathcal{L} , point processes are denoted by Φ , and a BLP typically consists of n_B lines unless specified otherwise. Capital math-font characters, e.g., Z , indicate random variables, with specific instances represented by lowercase letters, e.g., z . Scalar quantities are denoted by small letters, e.g., d . In the two-dimensional Euclidean plane, locations are bolded, e.g., \mathbf{x} . We use \mathbb{E} for expectation and \mathbb{P} for probability operators. For reference, additional notations can be found in Table III.

II. CHARACTERIZATION OF BLP AND BLCP

A. Binomial Line Process

A BLP \mathcal{L} is a finite collection of lines, i.e., n_B in the two-dimensional Euclidean plane. Formally,

$$\mathcal{L} \subset Q \triangleq \bigcup_{r \in [-R, R], \theta \in [0, \pi)} \{(x, y) \in \mathbb{R}^2 : x \cos \theta + y \sin \theta = r\}.$$

Notation	Description
\mathcal{L}	Binomial line process
L_i	i -th line of a BLP
R	Radius of circle in which BLP \mathcal{L} is generated
$\mathcal{B}((\theta, r), t)$	A disk of radius t centered at (θ, r)
n_B	Number of lines of the BLP \mathcal{L}
r_0	Distance of test point from the origin.
$l = r_0 \cos \theta - r$	Perpendicular distance of test point located at $(0, r_0)$ to a line (θ, r) .
$\mathcal{D}_B(r_0, t)$	Domain band corresponding to $\mathcal{B}((0, r_0), t)$
$A_D(r_0, t)$	Area of the domain bands corresponding to $\mathcal{B}((0, r_0), t)$
$\mathcal{V}_{\text{BLP}}(n_B, \mathcal{B})$	Void probability of the BLP with n_B lines on \mathcal{B}
$\mathcal{V}_{\text{BLCP}}(n_B, \mathcal{B})$	Void probability of the BLCP with n_B lines on \mathcal{B}
ρ_S	Density of length of chords/line segments in a bounded Borel set S
$\rho_i(w)$	Density of length of chords/line segments in the i -th annulus of equal width w
\mathcal{R} and $\rho(r)$	Line length measure and density
$\rho_{\times, i}(w)$	Density of intersections in the i -th annulus of equal width w
\mathcal{R}_{\times} and $\rho_{\times}(r)$	Intersection measure and density of BLP
$\rho_P(\lambda_{\text{PPP}})$	Intersection density of PLP
$A_{D_I}(r_0, t)$	Area of the domain bands corr. to the nearest intersection from the test point
Φ_i	1D PPP on L_i
λ	Intensity of Φ_i
$C(\theta, r)$	Length of a chord generated by a line corresponding to (θ, r) on $\mathcal{B}((0, r_0), t)$.
$\xi(r_0)$	SINR received at the test point
$p_S(\gamma)$	Success probability at threshold γ
$\mathcal{P}_M(\gamma, \beta)$	Meta distribution evaluated at SINR threshold γ and reliability threshold β

Table III: Summary of notations used in the paper.

Each line of \mathcal{L} corresponds to the point of a BPP defined on the finite cylinder $\mathcal{D} := [0, \pi) \times [-R, R]$. We call \mathcal{D} , the generating set or the domain set of \mathcal{L} , and a point $(\theta_i, r_i) \in \mathcal{D}$, corresponding to a line $L_i \in \mathcal{L}$, the generating point of L_i . The line segment is drawn from the origin to (θ_i, r_i) forms the normal to the line L_i . It should be noted that the generating points¹ do not form a BPP in $\mathcal{B}((0, 0), R)$ but rather in \mathcal{D} . Also, we see that regardless of the generating points forming a BPP in a cylinder \mathcal{D} in the representation space or in a disc $\mathcal{B}((0, 0), R)$ in the Euclidean plane, the resulting line process will always be non-homogeneous due to the finite domain of the generating set.

Furthermore, the BLP is a non-stationary process, and unlike stationary point processes (like PLP), the statistics of the BLP cannot be characterized from the perspective of a single typical point located, say, at the origin. However, due to the isotropic construction of the BLP, the properties of the BLP, as seen from a point, depend only on its distance from the origin and not its orientation. Accordingly, without loss of generality, we consider a test point located at $(0, r_0)$. Consider the line L_i and the disk $\mathcal{B}((0, r_0), t)$, all the points $(\theta_i, r_i) \in \mathcal{D}$ that result in L_i intersecting $\mathcal{B}((0, r_0), t)$, creates a set $\mathcal{D}_B(r_0, t)$ which we refer as *domain bands*. The area of $\mathcal{D}_B(r_0, t)$ to the total area of the generating set gives us the probability of a single intersecting $\mathcal{B}((0, r_0), t)$.

Lemma 1. *The probability that no line of the BLP intersects with $\mathcal{B}((0, r_0), t)$ is*

$$\mathcal{V}_{\text{BLP}}(n_B, \mathcal{B}((0, r_0), t)) = \left(\frac{2\pi R - A_D(r_0, t)}{2\pi R} \right)^{n_B},$$

¹The former would imply uniform location of points in the disk, while the latter correspond to uniform distances of the generating points between 0 and R .

where, n_B is the number of lines of \mathcal{L} and $A_D(r_0, t)$, the area of the so-called domain band is evaluated as

$$A_D(r_0, t) = \begin{cases} 2\pi t; & \text{for } r_0 + t \leq R \\ 2\pi t - 2r_0 \sqrt{1 - \left(\frac{R-t}{r_0}\right)^2} \\ \quad + 2(R-t) \cos^{-1}\left(\frac{R-t}{r_0}\right); & \text{for } r_0 + t > R \text{ and } r_0 - t \leq R \\ 2\pi t - 2r_0 \left(\sqrt{1 - \left(\frac{R-t}{r_0}\right)^2} - \sqrt{1 - \left(\frac{R+t}{r_0}\right)^2} \right) \\ \quad + 2(R-t) \cos^{-1}\left(\frac{R-t}{r_0}\right) \\ \quad - 2(R+t) \cos^{-1}\left(\frac{R+t}{r_0}\right); & \text{for } r_0 - t \geq R. \end{cases} \quad (1)$$

Thus, the CDF of the distance to the nearest line of the BLP from a test point at $(0, r_0)$ is $F_d(t) = 1 - \mathcal{V}_{\text{BLP}}(n_B, \mathcal{B}((0, r_0), t))$. For further details on the derivation and properties of domain bands, please refer to [29].

B. Binomial Line Cox Process

On each line L_i of \mathcal{L} , let us define an independent 1D PPP Φ_i with intensity λ . A BLCP Φ , is the collection of all such points on all lines of the BLP, i.e., $\Phi = \bigcup_{i=1}^{n_B} \Phi_i$. Thus, the BLCP is a doubly-stochastic or Cox process of random points defined on random lines. Similar to the BLP, the void probability of the BLCP w.r.t. to the location of the test point has been reported in [29]

Lemma 2. *The probability that the disk $\mathcal{B}((0, r_0), t)$ contains no points of Φ is given by*

$$\mathcal{V}_{\text{BLCP}}(n_B, \mathcal{B}((0, r_0), t)) = \left[\frac{1}{2\pi R} \int_0^{2\pi} \int_{r_0 \cos \theta - t}^{r_0 \cos \theta + t}$$

$$\exp(-\lambda C(\theta, r)) \, dr \, d\theta \Big]^{n_B},$$

where,

$$C(\theta, r) = \begin{cases} 2\sqrt{t^2 - l^2}; & t \geq |r_0 \cos \theta - r|, \\ 0; & \text{otherwise,} \end{cases}$$

is the length of the chord created by a line corresponding to $(\theta, r) \in \mathcal{D}$ in the disk $\mathcal{B}((0, r_0), t)$ and $l = |r_0 \cos \theta - r|$.

Following the void probability, the distance distribution of the nearest BLCP point from the test point $(0, r_0)$ is

$$F_{d_1}(t) = 1 - \mathcal{V}_{\text{BLCP}}(n_B, \mathcal{B}((0, r_0), t)). \quad (2)$$

Using a wireless network model with AP locations as BLCP points, the above result describes the distance distribution to the nearest AP. This will be utilized to calculate communication performance metrics in Section III.

C. Statistical properties of BLP

1) *Line Length Radial Density and Measure*: Recall that one of the objectives of studying the BLP is to emulate different densities of streets in the city center and the suburbs. The *line length radial density* and *line length radial measure* of the BLP provide new perspectives into the process's spatial distribution. Finding the ratio of the average length of lines within a disc to the area of a disk provides a way to calculate line length measure, which can then be used to determine the line length radial density. The analysis provides insights into the spatial variations of line lengths, which directly influence signal propagation, interference patterns, and connectivity. We define *line length radial measure* as,

Definition 1. The line length measure is $\mathcal{R}(S) = n_B \mathbb{E}(|L \cap S|_1)$, $S \subset \mathbb{R}^2$, where $|\cdot|_1$ is the Lebesgue measure in 1D and L is a line of the BLP. The corresponding radial density is

$$\rho(r) = \lim_{u \rightarrow 0} \frac{\mathcal{R}(\mathcal{B}((0, 0), r+u) \setminus \mathcal{B}((0, 0), r))}{\pi(2u + u^2)}.$$

The line length measure follows by integrating $\rho(r)$, i.e., $\mathcal{R}(S) = \int_S \rho(|\mathbf{x}|) \, d\mathbf{x}$, where $S \subset \mathbb{R}^2$. To study line length density, we first calculate the expected total chord length within a disk, i.e., the line length measure.

Theorem 1. For a BLP generated by n_B lines within a disk of radius R , the line length radial density at a distance r from origin is,

$$\rho(r) = \begin{cases} \frac{n_B}{2R}, & \text{if } r \leq R \\ \frac{n_B}{\pi R} \arcsin\left(\frac{R}{r}\right) & \text{if } r > R. \end{cases}$$

Proof. See Appendix A \square

The radial density $\rho(r)$ remains constant at $\frac{n_B}{2R}$ for $r \leq R$ and then decreases as $\mathcal{O}(1/r)$ as $r \rightarrow \infty$. We note that authors in [5] have derived the line density of PLP, which is defined as the mean line length per unit area. Now, although the metric of discussion is the same (line length density and the corresponding measure), the implications for urban planning

and wireless network dimensioning are vastly different. The major difference is that the line density for a PLP is constant throughout the Euclidean plane because of the homogeneity of PLP. In comparison, the line length radial density of BLP depends on the distance from the origin r .

The result of Theorem 1 can be used in modeling real-world road systems. By tuning its parameters, i.e., n_B and R , we can accurately emulate real data on the spatial density of roads. Likewise, emergency service providers can use this analysis to identify areas with low road density, making it difficult for emergency vehicles to reach certain locations quickly. In our current work, we use the result of Theorem 1 to determine the average number of potential targets detected by a radar.

2) *Radial Intersection Density*: Here, we study the point process formed by the intersections of the lines of the BLP. We introduce and characterize the intersection measure and the intersection density of the BLP. The analysis of *radial intersection density* in the context of the BLP not only offers insights into this specific model but also holds broader implications for the analysis of intersection patterns in various line processes. Understanding intersection density can help analyze traffic flow and congestion patterns in road networks, allowing transportation planners to identify potential bottlenecks and congestion-prone areas.

Theorem 2. The radial intersection density at a distance r from the origin for a BLP generated by n_B lines within a disk of radius R is

$$\rho_{\times}(r) = \begin{cases} \frac{n_B(n_B-1)}{4\pi R^2}, & \text{if } r \leq R, \\ \frac{n_B(n_B-1)}{4\pi^2 R^2 r} \left(2r \arcsin\left(\frac{R}{r}\right) - \frac{2R}{r} \sqrt{r^2 - R^2}\right) & \text{if } r > R. \end{cases} \quad (3)$$

Proof. See Appendix B \square

From (3), we see that intersection density first remains constant and then scales as $\mathcal{O}\left(\frac{1}{r}\right)$ as $r \rightarrow \infty$. By integrating the intersection density, we get the intersection measure

$$\mathcal{R}(S) = \int_S \rho_{\times}(|\mathbf{x}|) \, d\mathbf{x}, \quad S \subset \mathbb{R}^2.$$

Remark 1. The intersection measure in the \mathbb{R}^2 plane, as expected, is

$$\mathcal{R}_{\times} = \int_0^{2\pi} \int_0^{\infty} \rho_{\times}(r) \, r \, dr \, d\theta = \binom{n_B}{2} = \frac{n_B(n_B-1)}{2},$$

Lemma 3. The intersection density for a PLP with density λ_{PPP} is

$$\rho_{\text{P}}(\lambda_{\text{PPP}}) = \pi \lambda_{\text{PPP}}^2.$$

Proof. The proof follows from derivations similar to those in Theorem 2 but with the consideration of a Poisson distributed number of lines in S . We are omitting the proof as similar results have been derived by other papers. [30]. \square

Since the intersection density of a PLP remains constant regardless of the distance from the origin, it cannot capture the intricate spatial characteristics needed for real-world road network modeling. This uniform intersection density of the PLP doesn't reflect the complexities of actual road systems.

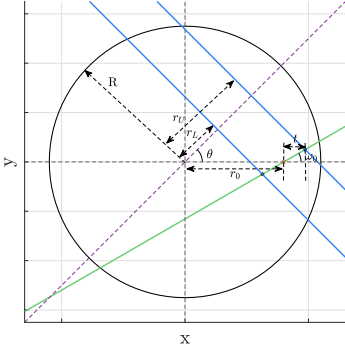


Fig. 2. Illustration of distances r_L and r_U (denoted by blue lines respectively) for a line (denoted by the green line) passing through $(0, r_0)$.

On the other hand, the BLP has a varying intersection density, making it a more realistic representation of real-world road networks. The result in Theorem 2 and Lemma 3 demonstrates this contrasting perspective between the BLP and PLP, respectively, highlighting the BLP's capacity to offer a more realistic and nuanced representation of road network patterns.

3) *Distance Distribution to the Nearest Intersection:* The distance distribution to the nearest intersection of BLP refers to a way of understanding how close intersections are to each other in a road network modeled using the BLP. In real-world road systems, vehicle charging points or bus stops are usually placed closer to intersections.

Consider a test point $(0, r_0)$ that lies on a line of the BLP. Consequently, $n_B - 1$ lines of the BLP intersect the line containing the test point almost surely. Let t be the distance to the nearest intersection from the test point. Also, let ω_0 be the angle formed between the line passing through $(0, r_0)$ and the x-axis. For an intersection to be located at a distance of t from the test point at an angle of ω_0 , there may exist a set of r for a given θ wherein no lines should be generated (see Fig. 2). Accordingly, to find the distance distribution, we need the set of all such (θ_i, r_i) for which lines $L_i \in \mathcal{L}$ do not intersect the line passing through $(0, r_0)$ at an angle of ω_0 within a distance of t from the test-point. For a given θ , the range of r where if a line is generated, intersects the test point within a distance t is $[r_L, r_U]$ calculated as:

$$r_L = \max \{-R, \min \{R, (r_0 \cos \theta - t |\cos(\theta - \omega_0)|)\}\} \quad (4)$$

$$r_U = \max \{-R, \min \{R, (r_0 \cos \theta + t |\cos(\theta - \omega_0)|)\}\} \quad (5)$$

The above equations of r_L and r_U are obtained using simple trigonometric calculations and include all possible cases for different values of r_0, t, θ , and ω_0 . As an example, the case presented in Fig. 2 corresponds to $\theta < \omega_0 + \frac{\pi}{2}$ and $\omega_0 < \frac{\pi}{2}$, accordingly, we have $r_L < r_U$. We see that when $\theta > \omega_0 + \frac{\pi}{2}$ we can end up with scenarios $r_L > r_U$, thus equation (4) and (5) have been defined in such a way that r_L will always be less than r_U for all possible values of r_0 and t . Also, (4) and (5) consider the cases when r_L and r_U exceed $[R, -R]$. Let D_I be the set of all such (θ, r) for which lines $L_i \in \mathcal{L}$ do not intersect the line passing through $(0, r_0)$ at an angle of ω_0 within a distance of t from the test-point. Fig. 3 shows some

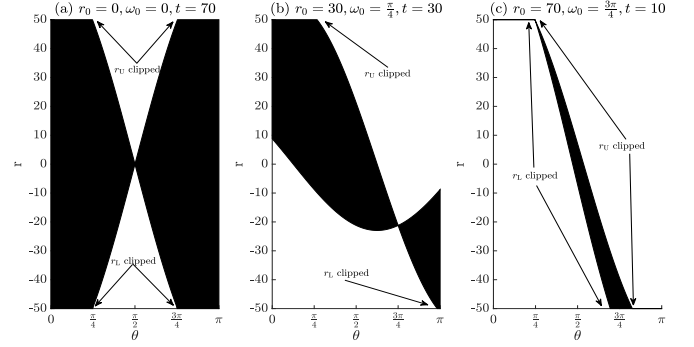


Fig. 3. Illustration of the region $D_I(r_0, t)$ for different values of r_0, ω_0 and t . Here $R = 50$.

examples of the domain band regions wherein a line should not be generated for it not to intersect the line passing through $(0, r_0)$ within a distance t from the test point at an angle of ω_0 . In Fig 3(a), as $r_0 = 0, \omega_0 = 0$ and $t > R$ we see that $|r_0| + t > R$, the domain bands are getting clipped at 50 and -50 for most of the initial and final values of θ . Likewise, in Fig. 3 (c), when the test point lies outside the circle of radius R and $t = 10$, i.e., $|r_0| - t > R$ and, more values of r_L and r_U are clipped for $\theta < \frac{\pi}{2}$ and the total width of the band is also small, thus showcasing that test points lying outside and having small t would experience fewer intersections.

Corollary 1. For a BLP line passing through $(0, r_0)$, the CDF of the distance d_I to the nearest intersection is

$$F_{d_I}(t) = 1 - \mathcal{V}_{B_I}(r_0, t).$$

The area of D_I for a BLP \mathcal{L} defined on $[0, 2\pi] \times [0, R]$ corresponding to $(0, r_0)$ and t is $A_{D_I}(r_0, t) = \int_0^\pi \int_0^\pi r_U d\theta d\omega_0 - \int_0^\pi \int_0^\pi r_L d\theta d\omega_0$. Accordingly, the probability that no line of the BLP intersects the line passing through $(0, r_0)$ within a distance t from the test point is $\mathcal{V}_{B_I}(r_0, t) = \left(1 - \frac{A_{D_I}(r_0, t)}{2\pi R}\right)^{n_B}$.

From Fig. 4, the nearest intersection is closer for greater n_B and lower r_0 values. A user near the origin can reach the nearest intersection in fewer steps than those outside the city center. These findings can aid in creating effective algorithms for reaching intersections where nearby bus stops or charging points are typically accessible.

D. Palm Perspective of the BLCP

Next, we study the BLCP from the perspective of a point of the process itself, using Palm calculus². Let us recall that for a PLCP Φ_{PLCP} with λ as the density of the points on the lines, we have $\mathbb{P}(\Phi_{\text{PLCP}} \in Y | o) = \mathbb{P}(\Phi_{\text{PLCP}} \cup \Phi_0 \cup \{o\} \in Y)$, where Φ_0 is a 1D PPP on a line that passes through the origin. In other words, the Palm distribution, i.e., conditioning on a point of the PLCP Φ_{PLCP} to be at the origin, is equivalent to adding (i) an independent Poisson process of intensity λ on a line through the origin with uniform independent angle and (ii) an atom at the origin to the PLCP. Similarly, for a BLCP, conditioning on a point to be located at \mathbf{x} is equivalent to considering an atom at \mathbf{x} , a 1D PPP on a line passing through

²In point process theory, the Palm probability refers to the probability measure conditioned on a point of the process being at a certain location [31].

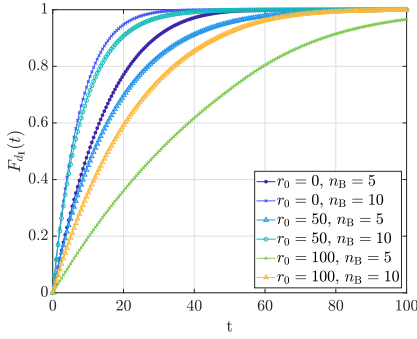


Fig. 4. Distance distribution to the nearest intersection from $(0, r_0)$.

\mathbf{x} and a BLCP Φ^1 defined on a BLP consisting of $n_B - 1$ lines in the same domain. Thus, the Palm measure of the BLCP can be expressed as follows.

Lemma 4. For a BLCP Φ defined on a BLP \mathcal{P} with n_B lines, we have

$$\mathbb{P}(\Phi \in Y \mid \mathbf{x} \in \Phi) = \mathbb{P}(\Phi^1 \cup \Phi_{\mathbf{x}} \cup \{\mathbf{x}\} \in \mathbf{Y}), \quad (6)$$

where $\Phi_{\mathbf{x}}$ is a 1D PPP on a randomly oriented line that passes through \mathbf{x} .

The applications of the Palm measure will be evident in the next section, where we employ the derived framework to analyze a wireless communication network. Prior to that, let us derive the PGFL of the shifted and reduced point process by conditioning on the location of the nearest point from the origin.

E. Probability Generating Functional

Here, we characterize the PGFL of the BLCP Φ . In this paper, we are interested in isotropic functions that depend only on the distance of the points from the origin, i.e., we consider functions of the form $f(\|\mathbf{x}\|)$.

Definition 2. Let \mathbf{x}_1 be the nearest point of a BLCP from $(0, r_0)$. Then, the shifted and reduced point process is defined as $\Phi' = \Phi - (0, r_0) \setminus \{\mathbf{x}_1\}$.

The motivation for studying the properties of Φ' in the context of wireless networks is as follows: if the AP locations are modeled as a BLCP, then Φ' represents the locations of the interfering APs from the perspective of a user located at a distance r_0 from the origin and connected to an AP located at a distance $\|\mathbf{x}_1\|$ from the user. The concept of shifting and reducing the point process to focus on a specific user's perspective introduces a unique aspect not commonly found in other line process models. In contrast, the PGFL of the PLCP typically deals with a stationary and homogeneous line process, making the derivation comparatively simpler. This differentiation showcases the BLCP's suitability for modeling real-world wireless networks, where user perspectives and specific interference scenarios play a crucial role. The following theorem characterizes the PGFL for the shifted and reduced BLCP Φ' .

Theorem 3. For a shifted and reduced BLCP $\Phi' = \Phi - (0, r_0) \setminus \{\mathbf{x}_1\}$ defined on a BLP with n_B lines generated

within $\mathcal{B}((0, 0), R)$, the PGFL of a function $f(r) = f(\|\mathbf{x}\|)$, conditioned on $d_1 = \|\mathbf{x}_1\|$ is given as

$$G(r_0, f(\cdot)) = \frac{1}{A_{\mathcal{D}}(r_0, d_1)} \iint_{\mathcal{D}_{\mathcal{B}}(0, d_1)} \exp\left(-2\lambda \int_{\sqrt{d_1^2 - l^2}}^{\infty} 1 - f\left(\sqrt{y^2 + l^2}\right) dy\right) dr d\theta \times \left(\frac{1}{2\pi R}\right)^{n_B - 1} \left(\iint_{\mathcal{D}_{\mathcal{B}}(0, d_1)} \exp\left(-2\lambda \int_{\sqrt{d_1^2 - l^2}}^{\infty} 1 - f\left(\sqrt{y^2 + l^2}\right) dy\right) dr d\theta + \iint_{\mathcal{D} \setminus \mathcal{D}_{\mathcal{B}}(0, d_1)} \exp\left(-2\lambda \int_0^{\infty} 1 - f\left(\sqrt{y^2 + l^2}\right) dy\right) dr d\theta \right)^{n_B - 1}.$$

where $d_1 = \|\mathbf{x}_1\|$ is the distance to the nearest point of $\Phi - (0, r_0)$ from the origin and $l = r_0 \cos \theta - r$. Consequently, the PGFL of Φ' is evaluated as $\mathbb{E}_{d_1}[G(r_0, f(\cdot))]$, where the distribution of d_1 is given by (2).

Proof. See Appendix C □

The PGFL serves as an analytical tool for understanding the behavior of BLCP-based wireless networks. Due to the non-stationary nature of the BLCP, we are able to characterize the SINR characteristics of a user conditioned on its location using the PGFL. In particular, we see that a city-center user may have a remarkably different network experience as compared to a suburban user from the same network deployment.

The fixed and deterministic number of lines in BLCP sets it apart as a less intricate and more straightforward case compared to PLCP. The fixed number of streets in BLCP leads to careful analysis of success probability. The line that contains the nearest AP has one set of interferers, and the other $n_B - 1$ lines have another set of interferers. Depending on the location of the test point, the line that contains the nearest AP changes as the test point moves from the origin to the outskirts of the city. The PGFL characterization takes care of these two different sets of interferers. Likewise, the performance of the test user also depends on its location, not only on the number of streets and the intensity of PPP. The number of streets will create a smaller or larger set of interferers, which affects the performance of the wireless network. From the user's perspective, the interest lies in understanding the mathematical assurances we can obtain when considering one's location within a city, particularly when comparing the success probability relative to their proximity to the city center versus the outskirts.

III. TRANSMISSION SUCCESS PROBABILITY IN WIRELESS NETWORKS

In wireless networks, several performance metrics are studied using the *transmission success probability*. It is the CCDF of the SINR over the fading coefficients and the spatial process of the locations of the APs. In this section, we define and characterize this metric using the results derived in the

previous sections. Instead of solely focusing on inventing new methods, this paper applies existing tools and concepts to a novel network architecture, i.e., BLCP. As a user, we want to know what kind of mathematical guarantee we can get if the user is at the city's center compared to the city's outskirts. Thus, having success probability as a function of r_0 , i.e., the distance of the test point from the origin, is quite a novel result which, according to our knowledge, cannot be found in any other line process models.

A. Success Probability - Definition

Let Φ be a point process (not necessarily a BLCP) consisting of points $\{\mathbf{x}_i\} \subset \mathbb{R}^2$, $i = 1, 2, \dots$. Consider a separate test point located at the origin. For convenience, let us assume that the points of Φ are ordered according to their distance from the origin, i.e., $\|\mathbf{x}_1\| \leq \|\mathbf{x}_2\| \leq \dots$. If the points of Φ emulate the locations of the APs relative to a receiver located at the origin, the receiver connects to the AP located at \mathbf{x}_1 . This is known as the nearest-AP association.

Each wireless link experiences fluctuations of the received power due to the constructive and destructive superposition of multiple reflecting paths in the propagation environment. This is termed small-scale fading. Classically, this impact is taken into account by multiplying the received signal with a random variable h with exponential distribution with parameter 1 [32]. For a path-loss exponent α , the SINR $\xi(r_0)$ is

$$\xi(r_0) = \frac{\xi_0 \|\mathbf{x}_1\|^{-\alpha} h_1}{1 + \xi_0 \sum_{\mathbf{x} \in \Phi \setminus \{\mathbf{x}_1\}} \|\mathbf{x}\|^{-\alpha} h_{\mathbf{x}}}, \quad (7)$$

where ξ_0 is a constant that considers the transmit power, AWGN noise, path-loss constant, and transmit and receive antenna gains. We assume that this parameter is the same for each transmit node. Typically, each $h_{\mathbf{x}}$ is independent of each other and identically distributed [32]. For the ease of notation, let us represent $\|\mathbf{x}_1\|$ by $d_{\mathbf{x}}$. Now, the transmission success probability at a threshold of γ is defined as the CCDF of $\xi(r_0)$: $p_S(\gamma) = \mathbb{P}[\xi(r_0) > \gamma]$ [32]. This represents the probability that an attempted transmission by the nearest AP located at \mathbf{x}_1 is decoded successfully by the receiver at the origin. In what follows, we refer to the transmission success probability as *success probability*.

B. Success probability for BLCP Locations of APs

The BLCP is a relevant model for studying deployment locations of APs along the streets of a city or, e.g., along alleyways of industrial warehouses. As discussed before, the network performance depends on the location of the test point². However, since the BLP is isotropic, we may infer that its properties, as seen from a point, only depend on its distance from the center, not its orientation. Accordingly, the test point can be considered to be located along the x-axis, i.e., we analyze the performance from the perspective of a test point located at $(0, r_0)$, without loss of generality. Equivalently,

²It may be noted that the wireless network performance analyzed at the test point referred here corresponds to the performance evaluated at the typical point at a location \mathbf{x} of a stationary receiver point process.

we can consider the receiver at the origin and study the statistics of the shifted point process $\Phi - (0, r_0)$. Recall that due to non-stationarity, this characterization allows us to study and contrast the performance of the users conditioned on their location. Let us assume that the receiver establishes a connection with its nearest AP (i.e., the nearest BLCP point from the receiver), consequently experiencing interference from all other APs. In such a case, the success probability is characterized by the following result.

Theorem 4. *For the network where locations of the APs are modeled as BLCP, the success probability for a receiver located at $(0, r_0)$ is given by*

$$p_S(\gamma) = \mathbb{E}_{d_1} \left[\exp \left(\frac{-\gamma}{\xi_0 d_1^{-\alpha}} \right) G \left(r_0, \frac{1}{1 + \frac{\gamma r^{-\alpha}}{d_1^{-\alpha}}} \right) \right],$$

where $G(r_0, f(\cdot))$ is given by Theorem 3.

Proof. See Appendix D □

The result of transmission success probability can be used to find the performance of the network with respect to the different parameters of the model like distance of the user from the center of the city r_0 , number of lines n_B , the intensity of 1D PPP on lines λ , etc. The mathematical expression of the success probability depends on the conditional probability distribution to the nearest BLCP point (2) and, more importantly, on the user's location r_0 . From the perspective of a network planner, Equation (15) provides an insight into the network performance depending on the location of the user, which is a novel concept yet to be seen in any other line process models. In Section IV, we will explore the delay and transmission density of the BLCP network.

Corollary 2. *For $\alpha = 2$ and $n_B = 1$, the PGFL of Φ' for the function $\frac{1}{1 + \frac{\gamma r^{-2}}{d_1^{-2}}}$ is given as*

$$G \left(r_0, \frac{1}{1 + \frac{\gamma r^{-2}}{d_1^{-2}}} \right) = \frac{1}{A_D(r_0, d_1)} \iint_{\mathcal{D}_B(0, d_1)} \exp \left(-2\lambda \frac{\gamma d_1^2}{\sqrt{\gamma d_1^2 + l^2}} \times \arctan \left(\sqrt{\frac{\gamma d_1^2 + l^2}{d_1^2 - l^2}} \right) \right) dr d\theta.$$

A single line in the BLCP is the simplest example of the aforementioned corollary. If $\alpha = 2$ is the path-loss constant in free space, a path-loss coefficient of 2 indicates normal signal attenuation with distance.

IV. APPLICATION - META DISTRIBUTION OF THE SINR IN BLCP

Although the success probability is a useful metric for planning a wireless network and tuning network parameters, it only provides an average view of the network across all possible realizations of Φ . This inhibits the derivation of a fine-grained view into the network. In this regard, the meta distribution, i.e., the distribution of the success probability conditioned on Φ provides a more refined framework [33], [34], allowing us to assess the coverage reliability under different

conditions. The CCDF of conditional success probability, i.e., $P_s(\gamma) = \mathbb{P}(\xi(r_0) \geq \gamma | \Phi)$ is a random variable due to Φ is called the meta distribution of the SINR, and is given as

$$\mathcal{P}_M(\gamma, \beta) = \mathbb{P}(P_s(\gamma) \geq \beta) = \mathbb{P}(\mathbb{P}(\xi(r_0) \geq \gamma | \Phi) \geq \beta).$$

which is a function of two parameters $\gamma \geq 0$ and $0 \leq \beta \leq 1$. In addition, consider another important aspect of wireless networks — not all transmitters transmit simultaneously but are controlled by an *access scheme*. In particular, let us assume a simple ALOHA access scheme wherein, when the connected AP transmits, each interfering AP transmits with a probability p [35]. Thus, each interference term is weighted by the probability of the corresponding node transmitting. Let the set of locations of the interfering nodes be denoted by $\mathcal{C} \subset \Phi'$. In this scheme, the conditional success probability can be obtained as

$$\begin{aligned} P_s(\gamma) &= \mathbb{P}(\xi(r_0) \geq \gamma | \Phi) \\ &= \mathbb{P}\left[\frac{\xi_0 d_1^{-\alpha} h_1}{1 + \xi_0 \sum_{\mathbf{x} \in \Phi'} h_{\mathbf{x}} d_{\mathbf{x}}^{-\alpha} \mathbf{1}(\mathbf{x} \in \mathcal{C})} \geq \gamma | \Phi\right] \\ &\stackrel{(a)}{=} \mathbb{E}_{h_{\mathbf{x}}}\left[\exp\left(\frac{-\gamma - \gamma \xi_0 \sum_{\mathbf{x} \in \Phi'} h_{\mathbf{x}} d_{\mathbf{x}}^{-\alpha} \mathbf{1}(\mathbf{x} \in \mathcal{C})}{\xi_0 d_1^{-\alpha}}\right)\right] \\ &= e^{\left(\frac{-\gamma}{\xi_0 d_1^{-\alpha}}\right)} \mathbb{E}_{h_{\mathbf{x}}}\left[\exp\left(\frac{-\gamma \xi_0 \sum_{\mathbf{x} \in \Phi'} h_{\mathbf{x}} d_{\mathbf{x}}^{-\alpha} \mathbf{1}(\mathbf{x} \in \mathcal{C})}{\xi_0 d_1^{-\alpha}}\right)\right] \\ &= e^{\left(\frac{-\gamma}{\xi_0 d_1^{-\alpha}}\right)} \left(\prod_{\mathbf{x} \in \Phi'} p \mathbb{E}_{h_{\mathbf{x}}}\exp\left(\frac{-\gamma \xi_0 d_{\mathbf{x}}^{-\alpha} h_{\mathbf{x}}}{\xi_0 d_1^{-\alpha}}\right) + 1 - p\right) \\ &\stackrel{(b)}{=} \exp\left(\frac{-\gamma}{\xi_0 d_1^{-\alpha}}\right) \left(\prod_{\mathbf{x} \in \Phi'} \frac{p}{1 + \frac{\gamma d_{\mathbf{x}}^{-\alpha}}{d_1^{-\alpha}}} + 1 - p\right). \end{aligned}$$

Step (a) is due to the exponential distribution of h_1 . Step (b) follows from the Laplace transform of the exponentially distributed $h_{\mathbf{x}}$. In general, it's not feasible to directly calculate the distribution of $P_s(\gamma)$. The standard way to tackle this difficulty is by computing its moments and transforming them to the distribution [36]. Analyzing the moments of $P_s(\gamma)$ provides valuable insights into the variability and distribution of successful transmissions. For example, it allows us to examine the mean local delay, indicating the anticipated number of transmissions needed for a successful communication event, which has direct relevance to latency-sensitive applications.

Theorem 5. *The b -th moment of $P_s(\gamma)$ conditioned on d_1 for any $b \in \mathbb{C}$ is given as*

$$\begin{aligned} M_b(d_1) &= e^{\frac{-b\gamma}{\xi_0 d_1^{-\alpha}}} \frac{1}{A_D(r_0, d_1)} \iint_{\mathcal{D}_B(0, d_1)} \exp\left(-2\lambda \int_{\sqrt{d_1^2 - l^2}}^{\infty} 1 - \right. \\ &\quad \left. \left(\frac{p d_1^{-\alpha}}{d_1^{-\alpha} + \gamma [y^2 + l^2]^{-\frac{\alpha}{2}}} + 1 - p\right)^b dy\right) dr d\theta \times \left(\frac{1}{2\pi R}\right)^{n_B - 1} \\ &\quad \left(\iint_{\mathcal{D}_B(0, d_1)} \exp\left(-2\lambda \int_{\sqrt{d_1^2 - l^2}}^{\infty} 1 - \left(\frac{p d_1^{-\alpha}}{d_1^{-\alpha} + \gamma [y^2 + l^2]^{-\frac{\alpha}{2}}}\right)^b\right) dr d\theta\right)^{n_B - 1} \end{aligned}$$

$$\begin{aligned} &+ 1 - p)^b dy) dr d\theta + \iint_{\mathcal{D} \setminus \mathcal{D}_B(0, d_1)} \exp\left(-2\lambda \int_0^{\infty} 1 - \right. \\ &\quad \left. \left(\frac{p d_1^{-\alpha}}{d_1^{-\alpha} + \gamma [y^2 + l^2]^{-\frac{\alpha}{2}}} + 1 - p\right)^b dy\right) dr d\theta \right)^{n_B - 1}, \end{aligned}$$

where $l = |r_0 \cos \theta - r|$. Taking an expectation over d_1 (see (2)) results in the unconditioned b -th moment.

Proof. We have

$$\begin{aligned} M_b &= \mathbb{E}_{\mathbf{x}_1}^! \left[\left(\exp\left(\frac{-\gamma}{\xi_0 d_1^{-\alpha}}\right) \prod_{\mathbf{x} \in \Phi'} \frac{p}{1 + \frac{\gamma d_{\mathbf{x}}^{-\alpha}}{d_1^{-\alpha}}} + 1 - p \right)^b \right] \\ &\stackrel{(c)}{=} \exp\left(\frac{-b\gamma}{\xi_0 d_1^{-\alpha}}\right) \mathbb{E}_{\mathbf{x}_1}^! \left[\left(\prod_{\mathbf{x} \in \Phi'} \left(\frac{p}{1 + \frac{\gamma d_{\mathbf{x}}^{-\alpha}}{d_1^{-\alpha}}} + 1 - p \right)^b \right) \right] \\ &\stackrel{(d)}{=} \exp\left(\frac{-b\gamma}{\xi_0 d_1^{-\alpha}}\right) \frac{1}{A_D(r_0, d_1)} \iint_{\mathcal{D}_B(0, d_1)} \exp\left(-2\lambda \int_{\sqrt{d_1^2 - l^2}}^{\infty} 1 - \right. \\ &\quad \left. \left(\frac{p d_1^{-\alpha}}{d_1^{-\alpha} + \gamma [y^2 + l^2]^{-\frac{\alpha}{2}}} + 1 - p\right)^b dy\right) dr d\theta \times \left(\frac{1}{2\pi R}\right)^{n_B - 1} \\ &\quad \left(\iint_{\mathcal{D}_B(0, d_1)} \exp\left(-2\lambda \int_{\sqrt{d_1^2 - l^2}}^{\infty} 1 - \left(\frac{p d_1^{-\alpha}}{d_1^{-\alpha} + \gamma [y^2 + l^2]^{-\frac{\alpha}{2}}}\right)^b\right) dr d\theta + \iint_{\mathcal{D} \setminus \mathcal{D}_B(0, d_1)} \exp\left(-2\lambda \int_0^{\infty} 1 - \right. \right. \\ &\quad \left. \left. \left(\frac{p d_1^{-\alpha}}{d_1^{-\alpha} + \gamma [y^2 + l^2]^{-\frac{\alpha}{2}}} + 1 - p\right)^b dy\right) dr d\theta\right)^{n_B - 1}. \quad (8) \end{aligned}$$

Step (c) follows because the expectation is over Φ' . Step (d) follows from the PGFL of the BLCF. \square

Then, the meta distribution of the SINR is calculated using the Gil-Palaez theorem as [37]

$$F_{P_s}(z) = \frac{1}{2} + \frac{1}{\pi} \int_0^{\infty} \frac{\Im(e^{-ju \log(z)} M_{ju})}{u} du,$$

where $\Im(\cdot)$ denotes the imaginary part, and $j^2 = -1$.

The capacity of a wireless network can be studied in terms of the successful transmission density $p\lambda M_1$. Here M_1 is the 1st moment of $P_s(\gamma)$, essentially the transmission success probability. We see that once we take the mean of $P_s(\gamma)$, the only source of randomness left in $P_s(\gamma)$, i.e., spatial randomness is removed, and we get the $p_s(\gamma)$. Therefore, when we multiply M_1 with λ , we get the total number of successful transmissions, and when p is also multiplied, we get the average number of successful transmissions. This metric informs us about the density of simultaneous successful transmissions, offering insights into the network's ability to handle multiple connections efficiently. Furthermore, the mean local delay is

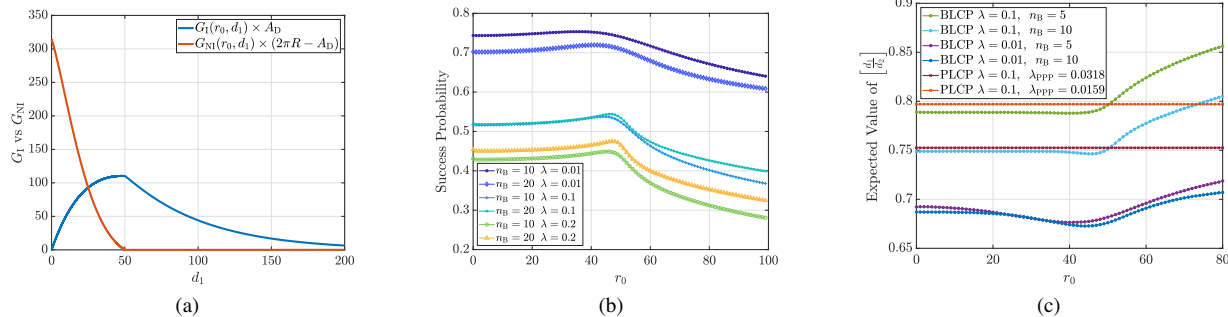


Fig. 5. (a) Conditional PGFL of intersecting and non-intersecting lines (see (13)). Here $r_0 = 0$, $R = 50$, $\lambda = 0.1$ and $n_B = 10$, (b) Success probability with respect to r_0 , and (c) $\mathbb{E}\left[\frac{d_1}{d_2}\right]$ with respect to r_0 .

the expected number of transmissions required for successful transmission. It is obtained by setting $b = -1$ [37]. We see that M_{-1} is the first negative moment of $P_s(\gamma)$. The inverse mean of $P_s(\gamma)$ analyzes the expected number of transmissions to get the first successful full transmission. The product of M_{-1} and $1/p$, is called mean local delay, a crucial parameter in latency-constrained networks.

Corollary 3. For $\alpha = 2$, the mean local delay conditioned on d_1 is $\mathcal{D}(p) = \frac{1}{p} M_{-1}$, where

$$M_{-1} = \exp\left(\frac{\gamma}{\xi_0 d_1^\alpha}\right) \times \frac{1}{A_D(r_0, d_1)} \iint_{\mathcal{D}_B(0, d_1)} \exp\left(2\lambda \frac{p\gamma d_1^2}{\sqrt{\gamma d_1^2(1-p) + l^2}} \times \arctan\left(\sqrt{\frac{\gamma d_1^2(1-p) + l^2}{d_1^2 - l^2}}\right)\right) drd\theta$$

$$\times \left(\frac{1}{2\pi R}\right)^{n_B-1} \left(\iint_{\mathcal{D}_B(0, d_1)} \exp\left(2\lambda \frac{p\gamma d_1^2}{\sqrt{\gamma d_1^2(1-p) + l^2}} \times \arctan\left(\sqrt{\frac{\gamma d_1^2(1-p) + l^2}{d_1^2 - l^2}}\right)\right) drd\theta + \iint_{\mathcal{D} \setminus \mathcal{D}_B(0, d_1)} \exp\left(\lambda \frac{p\pi\gamma d_1^2}{\sqrt{\gamma d_1^2(1-p) + l^2}}\right) drd\theta \right)^{n_B-1}.$$

In the next section, we discuss how optimizing the channel access probability p to minimizing the mean local delay is non-trivial due to the impact of interference. In essence, we will see how Theorem 5 facilitates a nuanced understanding of transmission density and latency across different locations within the network. As users move through urban landscapes characterized by varying access point densities and interference patterns, their latency experiences fluctuate.

V. NUMERICAL RESULTS AND DISCUSSION

In this section, we discuss some numerical results to highlight the applications of the derived framework in analyzing the wireless network. Unless otherwise stated, all results are for $R = 50$, $\alpha = 2$, $\xi_0 = 2.9858 \cdot 10^{-8}$, and $\gamma = 0.1$.

A. On the Success Probability

First, let us observe some features of the weighted conditional PGFLs for the function $f(r) = \frac{1}{1+\gamma(d_1/r)^\alpha}$ as derived in (13)). From (14) note that these conditional PGFLs constitute the overall functional $G(r_0, f(\cdot))$, i.e.,

$$G(r_0, f(\cdot)) = G_I(r_0, d_1) \left(\frac{1}{2\pi R}\right)^{n_B-1} (A_D(r_0, d_1) G_I(r_0, d_1) + (2\pi R - A_D(r_0, d_1)) G_{NI}(r_0, d_1))^{n_B-1}.$$

Moreover, since p_S is proportional to $G(r_0, f(\cdot))$ for a given d_1 , it is important to study the trends in the weighted conditional PGFLs with d_1 . For lower values of d_1 , $\mathcal{D}_B(0, d_1)$ is smaller than $\mathcal{D} \setminus \mathcal{D}_B(0, d_1)$. Accordingly, Fig. 5a shows that $(2\pi R - A_D(0, d_1))G_{NI}(0, d_1)$ has a value $2\pi R = 314.15$ at $d_1 = 0$ and decreases with d_1 until it becomes zero exactly at $d_1 = 50$. This is because all lines intersect the disk at $d_1 = R$. On the contrary, $A_D(0, d_1)G_I(0, d_1)$ has a value 0 at $d_1 = 0$ and increases till $d_1 = 50$, as the area corresponding to intersecting lines increases. Beyond $d_1 = 50$, $A_D(0, d_1)G_I(0, d_1)$ decreases precisely due to the increasing distance of the serving AP from the receiver.

In Fig. 5b, we plot the success probability with respect to r_0 for different values of λ and n_B . We observe that the success probability first increases slightly with r_0 , reaches a maximum, and starts decreasing. To delve deeper into this phenomenon, we plot the expected value of the ratio of the distance from the nearest BLCP point to the distance of the second nearest BLCP point with respect to r_0 . In systems where the nearest interferer contributes most of the interference power, this parameter is a good indicator of the success probability. From Fig. 5c, we note that the value of $\mathbb{E}\left[\frac{d_1}{d_2}\right]$ decreases with r_0 at first, reaches its minimum value near $r_0 = R$ and increases beyond that. This indicates that as we move away from the city center, both the serving AP and the interferers become statistically distant from the test point, the relative increase in d_1 is higher as compared to the relative increase in d_2 with r_0 . In case the streets follow a BLCP, such an insight for urban networks cannot be obtained with PLCP models (also shown in Fig. 5c).

B. Optimal Network Parameters

In Fig. 6a and Fig. 6b-6c, we plot the success probability with respect to λ and n_B respectively for different values of

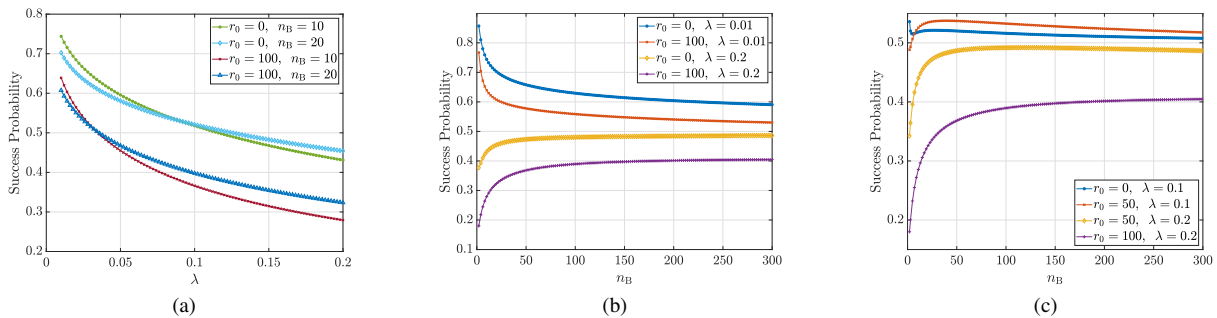


Fig. 6. (a) Success probability with respect to the density of APs. (b) and (c) Success probability with respect to n_B .

r_0 . Fig. 6a shows that as λ increases, the success probability decreases due to the increase in interference. Irrespective of the location of the test point after a certain λ value, more streets provide a higher success probability than fewer streets. For value of $\lambda < 0.05$, $n_B = 10$ provide better success probability than $n_B = 20$ and vice-versa for $\lambda > 0.05$. Likewise in Fig 6b we see that for $\lambda = 0.2$, success probability increases as n_B increases, while for $\lambda = 0.01$, success probability decreases as n_B increases. This shows that with a high number of APs, complemented with larger n_B provides better coverage as compared to smaller n_B . Eventually, success probability saturates as n_B increases because the nearest transmitter and nearest interferer are nearly at the same distance to the test point. Based on the test device's location, an optimal deployment density of the APs may exist for which $p_s(\gamma)$ is maximum for parameters such as n_B , transmit power, etc.

In Fig. 6c, we plot the success probability with respect to n_B but for higher values of λ . We observe that n_B maximizes the success probability for some values of r_0 and λ . For example, when $r_0 = \{0, 50\}$ (i.e., at the center and city edge), and $\lambda = \{0.1, 0.2\}$, the success probability first increases and then decreases. At the same time, when the test point is at the outskirts, i.e., $r_0 = 100$, the success probability keeps increasing. This suggests that increasing the number of lines may increase or decrease the probability of success depending on the test device's location and deployment density.

C. Comparison with non-homogeneous Cox models

In Fig. 7, we plot the success probability for r_0 for three new Cox process models and homogeneous PLCP. Recall that due to the non-homogeneous nature of the BLCP, a fair comparison must be drawn with respect to other non-homogeneous models. In light of this, we introduce three additional, non-homogeneous models. First, we introduce the E1-PLCP model, which is constructed by thinning PLCP points based on their distance from the origin using an exponential decay function, $f(x) = \exp(-\delta x)$, where x represents the point's distance from the origin and δ is the decay factor. The modified E1-PLCP has more points around a certain radius, and the average number of points decreases as we move out. Likewise, E2-PLCP models the intensity of the line process using an exponential-based intensity function, $\lambda(r) = \exp(-\delta r)$, where r is the perpendicular distance of a PLCP line from the origin. Consequently, the average number of lines generated decreases as one moves away from the city

center. In E-BLCP, an additional layer of randomness is added to the BLCP model by generating non-homogeneous PPPs on each line with intensity function $\lambda(x) = \exp(-\delta x)$, where x denotes the distance of a BLCP point from the generating point of its respective line. This results in a more realistic distribution of points concentrated around the city center, enhancing the realism of the original BLCP model.

Fig. 7 shows that for BLCP and E-BLCP, the success probability initially rises with r_0 , peaks, and then decreases. BLCP behavior is detailed in the previous subsection, where the expected distance between the nearest AP and the nearest interferer falls and eventually increases. The point of minimum value of $\mathbb{E}\left[\frac{d_1}{d_2}\right]$ is the same as the value where success probability is maximum. In E-BLCP, the non-homogeneous intensity function leads to a higher success probability than BLCP but has the same behavior. The higher success probability can be attributed to the reduced number of average BLCP points within and outside the city circle. As the average number of E-BLCP points decreases exponentially, the success probability rate decreases when the test point's location is smaller than that of BLCP. In the case of homogeneous PLCP, the probability of success is constant at all locations. Now, coming to the remaining two non-homogeneous PLCP models, the probability of success keeps decreasing with r_0 . The continuous decrease of E1-PLCP and E2-PLCP is because the average number of cox points in both processes is decreasing with respect to the origin. In the case of BLCP, the average number of points first remains constant up to the city circumference and then decreases. Let's consider a test point around the city edge; in the case of BLCP, towards the city center, the average number of interferers is constant, and towards the city outskirts, the average number of interferes is decreasing. The test point at this location has the optimum distance to the nearest AP and the nearest interferer. From the perspective of this location, as we move inside the city, the distance to the nearest interferer increases, and as we move out, the distance to the nearest AP and nearest interferer increases at such a rate that the probability of success decreases. This spatial behavior of cox points cannot be seen in E1-PLCP and E2-PLCP; thus, success probability decreases as r_0 increases.

D. Results on Moments of Conditional Success Probability and Meta Distribution

Fig. 8a shows the mean local delay for a test node at the origin. As the transmit probability increases, initially,

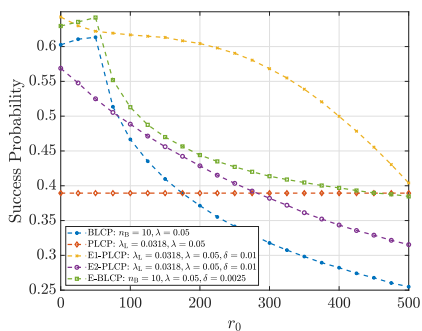


Fig. 7. Comparison of success probability with respect r_0 for BLCP, PLCP, E1-PLCP, E2-PLCP, and E-BLCP.

the local delay decreases since the transmitter accesses the channel more frequently. However, as the transmit probability increases, a higher density of interfering APs results in the deterioration of the coverage and an increase in the delay. Thus, an optimal transmit probability exists for minimizing the delay, which is non-trivial to derive due to the two contending phenomena - increasing p i) increases the frequency with which the service to the test device is attempted, thereby reducing the delay and ii) increases the interference which reduces the transmission success and increases the delay. Such nuances of the wireless network are kept for future study.

Fig. 8b shows the successful transmission density, $p\lambda M_1$, which is the number of successful transmissions per unit area. This acts as an indicator of the network capacity. Here we have assumed $R = 50$, $n_B = 10$, and $\gamma = -10$ dB. We see that $p\lambda M_1$ increases as p increases, specifying that more transmission leads to better transmission density. As we move closer to the city edge, i.e., $r_0 = 50$, successful transmission density increases slightly compared to $r_0 = 0$ due to reduced interference. However, at a further distance from the city center, the successful transmission density decreases due to the increasing distance from the serving AP. This is consistent with the results of Fig. 5b where we see that as r_0 increases, coverage first increases and then decreases. Such network characteristics as a function of r_0 cannot be obtained using classical models such as PLP and PLCP.

The optimal transmit probability for minimizing the mean local delay is plotted in Fig. 8c for different locations of the test node, R , λ , and n_B . We observe that as r_0 increases, p^* increases first and then decreases. We see that the maximum value of p^* occurs near the edge of the domain of the BLP. As r_0 increases further, the distance to the nearest transmitter and the other interfering nodes increases. Consequently, the transmit probability is reduced to limit the device outage. Interestingly, for $r_0 \leq 30$, p^* for $n_B = 10$ is higher as compared to $n_B = 20$ since the lines are densely packed around the city center. On the contrary, for $r_0 \geq 30$, $n_B = 20$ needs a higher p values than the case with $n_B = 10$.

The meta distribution of the success probability is plotted in Fig. 8d with respect to the reliability threshold β , for $R = 50$ and $r_0 = 0$. We observe that for an SINR threshold of $\gamma = -20$ dB, most users are under coverage with a reliability of 70% (or probability 0.7). On the contrary, for a service characterized by $\gamma = 0$ dB, with a 90% guarantee, it can be

claimed that none of the users will be under coverage. For $\gamma = -10$ dB, we see that there is a near-linear relationship between the reliability and the number of users under coverage.

VI. CONCLUSIONS AND FUTURE WORK

We have characterized the binomial line Cox process (BLCP), which takes into account the non-homogeneity of lines in an Euclidean plane. Although several line processes are studied in the literature, none of the existing models consider the non-homogeneity of the lines. This is a drawback of the existing models since practical problems, e.g., wireless network planning or transport infrastructure planning, need to deal with non-homogeneous streets in a city. We derive the line length radial density and intersection density, which help us visualize varying street densities. We also derive the distribution to the distance of the nearest intersection, the probability generating functional of the BLCP, and used it to analyze the transmission success probability in a wireless network. Then, we have provided extensive numerical results to derive system design insights for such network deployments. Furthermore, we have characterized the meta distribution of the SINR in order to gain a fine-grained view of the network. We envisage that the statistical model developed in this paper will be employed to study practical problems involving urban street planning. The shortest path length, E1-BLCP, and non-homogeneous PLCP are interesting research directions that will be taken up in future work.

REFERENCES

- [1] M. T. Shah, "Codes for BLP and BLCP: Statistical characterization and applications in wireless network analysis." Github, <https://github.com/mt19146/blcp>, 2023.
- [2] M. T. Shah, G. Ghatak, S. Sanyal, and M. Haenggi, "Analyzing wireless networks using binomial line cox processes," in *2023 21st International Symposium on Modeling and Optimization in Mobile, Ad Hoc, and Wireless Networks (WiOpt)*, pp. 1–8, IEEE, 2023.
- [3] B. Ripley, "The foundations of stochastic geometry," *The Annals of Probability*, vol. 4, no. 6, pp. 995–998, 1976.
- [4] F. Baccelli *et al.*, "Stochastic geometry and architecture of communication networks," *Telecommunication Systems*, vol. 7, no. 1, pp. 209–227, 1997.
- [5] H. S. Dhillon and V. V. Chetlur, "Poisson line Cox process: Foundations and applications to vehicular networks," *Synthesis Lectures on Learning, Networks, and Algorithms*, vol. 1, no. 1, pp. 1–149, 2020.
- [6] G. Mansfield, "Using Streetlights to Boost 5G Deployments in Cities," <https://about.att.com/innovationblog/2022/streetlights-to-boost-5g-deployments.html>, February 25, 2022.
- [7] "NYC allows 5G equipment on streetlamps," <https://www.fiercewireless.com/5g/nyc-allows-5g-equipment-streetlamps>, 2020.
- [8] C. Gloaguen, F. Fleischer, H. Schmidt, and V. Schmidt, "Fitting of stochastic telecommunication network models via distance measures and monte-carlo tests," *Telecommunication Systems*, vol. 31, pp. 353–377, 2006.
- [9] F. Morlot, "A population model based on a Poisson line tessellation," in *2012 10th International Symposium on Modeling and Optimization in Mobile, Ad Hoc and Wireless Networks (WiOpt)*, pp. 337–342, 2012.
- [10] W. S. Kendall, "From random lines to metric spaces," *The Annals of Probability*, vol. 45, no. 1, pp. 469–517, 2017.
- [11] J. Kahn, "Improper Poisson line process as SIRS in any dimension," *The Annals of Probability*, vol. 44, no. 4, pp. 2694–2725, 2016.
- [12] J. P. Jeyaraj and M. Haenggi, "Cox models for vehicular networks: SIR performance and equivalence," *IEEE Transactions on Wireless Communications*, vol. 20, no. 1, pp. 171–185, 2020.
- [13] M. J. Farooq *et al.*, "A stochastic geometry model for multi-hop highway vehicular communication," *IEEE Transactions on Wireless Communications*, vol. 15, no. 3, pp. 2276–2291, 2015.

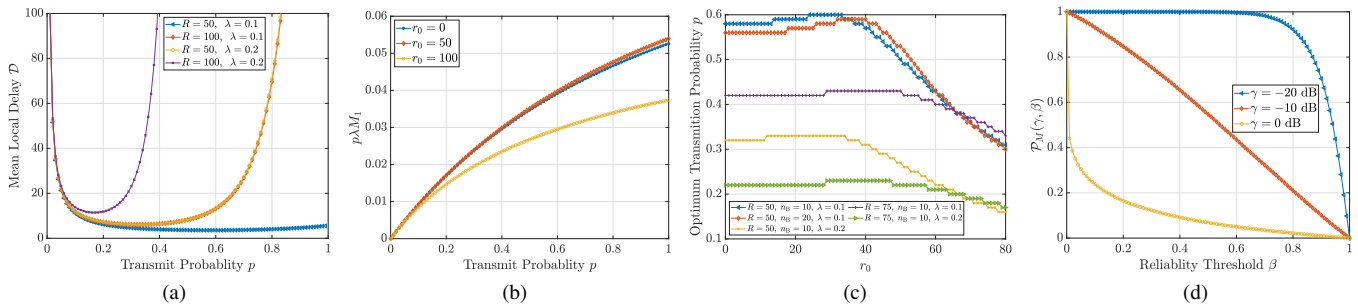


Fig. 8. (a) Mean local delay with respect to the transmit probability for different values of R and λ . Here, $r_0 = 0$. (b) Successful transmission density. (c) Optimal transmit probability for minimizing the mean local delay. (d) SINR meta distribution.

- [14] N. Chenavier and R. Hemsley, "Extremes for the inradius in the Poisson line tessellation," *Advances in Applied Probability*, vol. 48, no. 2, pp. 544–573, 2016.
- [15] Q. Cui, N. Wang, and M. Haenggi, "Vehicle distributions in large and small cities: Spatial models and applications," *IEEE Transactions on Vehicular Technology*, vol. 67, no. 11, pp. 10176–10189, 2018.
- [16] G. Ghatak, A. De Domenico, and M. Coupechoux, "Small cell deployment along roads: Coverage analysis and slice-aware rat selection," *IEEE Transactions on Communications*, vol. 67, no. 8, pp. 5875–5891, 2019.
- [17] C.-S. Choi and F. Baccelli, "An analytical framework for coverage in cellular networks leveraging vehicles," *IEEE Transactions on Communications*, vol. 66, no. 10, pp. 4950–4964, 2018.
- [18] C.-S. Choi and F. Baccelli, "Poisson cox point processes for vehicular networks," *IEEE Transactions on Vehicular Technology*, vol. 67, no. 10, pp. 10160–10165, 2018.
- [19] C.-S. Choi and F. Baccelli, "A stochastic geometry model for spatially correlated blockage in vehicular networks," *IEEE Internet of Things Journal*, vol. 9, no. 20, pp. 19881–19889, 2022.
- [20] C.-S. Choi, "User association in a heterogeneous vehicular network with roadside units and vehicle relays," *IEEE Wireless Communications Letters*, vol. 11, no. 11, pp. 2345–2349, 2022.
- [21] C.-S. Choi and F. Baccelli, "Los coverage area in vehicular networks with cox-distributed roadside units and relays," *IEEE Transactions on Vehicular Technology*, 2023.
- [22] V. V. Chetlur and H. S. Dhillon, "Coverage analysis of a vehicular network modeled as cox process driven by poisson line process," *IEEE Transactions on Wireless Communications*, vol. 17, no. 7, pp. 4401–4416, 2018.
- [23] V. V. Chetlur and H. S. Dhillon, "Coverage and rate analysis of downlink cellular vehicle-to-everything (C-V2X) communication," *IEEE Transactions on Wireless Communications*, vol. 19, no. 3, pp. 1738–1753, 2019.
- [24] V. V. Chetlur and H. S. Dhillon, "On the load distribution of vehicular users modeled by a Poisson line Cox process," *IEEE Wireless Communications Letters*, vol. 9, no. 12, pp. 2121–2125, 2020.
- [25] V. V. Chetlur, H. S. Dhillon, and C. P. Dettmann, "Shortest path distance in manhattan poisson line cox process," *Journal of Statistical Physics*, vol. 181, pp. 2109–2130, 2020.
- [26] K. Pandey, K. R. Perumalla, A. K. Gupta, and H. S. Dhillon, "Fundamentals of vehicular communication networks with vehicle platoons," *IEEE Transactions on Wireless Communications*, 2023.
- [27] J. P. Jeyaraj, M. Haenggi, A. H. Sakr, and H. Lu, "The transdimensional poisson process for vehicular network analysis," *IEEE Transactions on Wireless Communications*, vol. 20, no. 12, pp. 8023–8038, 2021.
- [28] T. Courtat, C. Gloaguen, and S. Douady, "Mathematics and morphogenesis of cities: A geometrical approach," *Phys. Rev. E*, vol. 83, p. 036106, Mar 2011.
- [29] G. Ghatak, "Binomial line processes: Distance distributions," *IEEE Transactions on Vehicular Technology*, vol. 71, no. 2, pp. 2176–2180, 2022.
- [30] R. Schneider and W. Weil, *Stochastic and integral geometry*, vol. 1. Springer, 2008.
- [31] M. Haenggi, *Stochastic geometry for wireless networks*. Cambridge University Press, 2012.
- [32] M. Haenggi *et al.*, "Stochastic geometry and random graphs for the analysis and design of wireless networks," *IEEE Journal on Selected Areas in Communications*, vol. 27, no. 7, pp. 1029–1046, 2009.
- [33] M. Haenggi, "Meta distributions - Part 1: Definition and examples," *IEEE Communications Letters*, vol. 25, no. 7, pp. 2089–2093, 2021.
- [34] M. Haenggi, "Meta distributions - Part 2: Properties and interpretations," *IEEE Communications Letters*, vol. 25, no. 7, pp. 2094–2098, 2021.
- [35] N. Abramson, "The aloha system: Another alternative for computer communications," in *Proceedings of the November 17-19, 1970, Fall Joint Computer Conference, AFIPS '70 (Fall)*, pp. 281–285, Association for Computing Machinery, 1970.
- [36] X. Wang and M. Haenggi, "Fast hausdorff moment transforms for meta distributions in wireless networks," *IEEE Transactions on Wireless Communications*, 2023.
- [37] M. Haenggi, "The meta distribution of the SIR in Poisson bipolar and cellular networks," *IEEE Transactions on Wireless Communications*, vol. 15, no. 4, pp. 2577–2589, 2016.

APPENDIX A PROOF OF THEOREM 1

Proof. Let $S = \mathcal{B}((0, r_0), t)$. We have

$$\mathcal{R}(S) = \mathbb{E}[K \bar{L}_1] = \bar{L}_1 \mathbb{E}[K] = \bar{L}_1 n_B \left(\frac{A_D(r_0, t)}{2\pi R} \right), \quad (9)$$

where K is the number of lines intersecting disk $\mathcal{B}((0, r_0), t)$ and is binomial distributed. \bar{L}_1 is the expected length of the chord formed by a single line in the disk S . For $\mathcal{B}((0, r_0), t)$, \bar{L}_1 is evaluated as $\bar{L}_1 = \frac{1}{A_D(r_0, t)} \iint_{A_D} 2\sqrt{(t^2 - l^2)} dr d\theta$, where

$A_D(r_0, t)$ is obtained from (1). Next, we consider concentric circles centered at the origin having radii $l = \{w, 2w, \dots\}$. In the i -th annulus of width w , the average length of line segments given by (9) to the area of the annulus gives the line length density $\rho_i(w)$ as

$$\rho_i(w) = \begin{cases} \frac{n_B}{2R}; & \text{for } (i+1)w \leq R, \\ \frac{n_B}{\pi w^2 (2i+1)} \left(\left(\sqrt{(i+1)^2 w^2 - R^2} + \arcsin\left(\frac{R}{(i+1)w}\right) \times \frac{(i+1)^2 w^2}{R} \right) - \left(\sqrt{i^2 w^2 - R^2} + \arcsin\left(\frac{R}{iw}\right) \times \frac{i^2 w^2}{R} \right) \right); & \text{for } (i+1)w > R. \end{cases} \quad (10)$$

Leveraging this, we can characterize the line length radial density of the BLP as a limiting function of the density in annuli. Precisely, the theorem statement is obtained by substituting $iw = r$ and taking the limit $w \rightarrow 0$ in (10). \square

APPENDIX B PROOF OF THEOREM 2

Let $S = \mathcal{B}((0, 0), t)$, and consider a BLP line L_0 generated at the point $(0, r_0)$ where $0 \leq r_0 \leq \min\{t, R\}$.

First, we determine the domain band \mathcal{D}_\times corresponding to the intersection on L_0 i.e., all such (θ_i, r_i) for which lines $L_i \in \mathcal{L}$ will intersect line L_0 within S . For a given θ , the range of r where if a line is generated intersects $(0, r_0)$ within S is, $\max \left\{ -R, \left(r_0 \cos \theta - \sqrt{t^2 - r_0^2} \sin \theta \right) \right\} \leq r_i \leq \min \left\{ R, \left(r_0 \cos \theta + \sqrt{t^2 - r_0^2} \sin \theta \right) \right\}$. For $t > R$, the domain band gets clipped to R (upper) and $-R$ (lower) limits; thus, the area of the domain band for these two cases is,

Case 1: $t \leq R$. Here $S \subset \mathcal{B}((0, 0), R)$. Consequently, there is no clipping in the values of r , and the area of \mathcal{D}_\times is averaged for r_0 , uniformly distributed between 0 and t .

Case 2: $t > R$. Here $\mathcal{B}((0, 0), R) \subset S$. Accordingly, the values of r are limited to R and $-R$. The values of θ for which r are clipped are obtained by solving for θ in the equations $r_0 \cos \theta - \sqrt{t^2 - r_0^2} \sin \theta = -R$ and $r_0 \cos \theta + \sqrt{t^2 - r_0^2} \sin \theta = R$, respectively.

Thus, within these limits of θ , the area of the domain band for a line to intersect the line L_0 within S is

$$A_{\mathcal{D}_\times}(t) = \begin{cases} \pi t, & \text{if } t \leq R, \\ \frac{2}{R} \left(t^2 \arcsin \left(\frac{R}{t} \right) + 2R^2 \arccos \left(\frac{R}{t} \right) - \sqrt{t^2 - R^2} \right) & \text{if } t > R. \end{cases}$$

Accordingly, the probability that a line intersects a single line within S is obtained as $\mathcal{P}_\times(t) = \frac{A_{\mathcal{D}_\times}(t)}{2\pi \min\{t, R\}}$. Now, let us assume that k lines are generated in S . Each of these intersects L_0 with probability $\mathcal{P}_\times(t)$. As a result, the average number of intersections on L_0 within S from the k lines is

$$\mathcal{N}' = \sum_{j=0}^k j \binom{k}{j} (\mathcal{P}_\times(t|t \leq R))^j (1 - \mathcal{P}_\times(t|t \leq R))^{k-j} = \frac{k}{2}.$$

Finally, in order to determine the average number of intersections on all the lines within S , we take the expectation over the number of lines generated within S . This is evaluated as

$$\mathcal{N}_1 = \sum_{k=0}^{n_B-1} \underbrace{\binom{n_B}{k+1}}_{T_1} \underbrace{\left(\frac{t}{R} \right)^{k+1} \left(1 - \frac{t}{R} \right)^{n_B-k-1}}_{T_2} \times \underbrace{\frac{k}{2}}_{T_3} \times \underbrace{(k+1)}_{T_4} \times \underbrace{\frac{1}{2}}_{T_5} = \frac{n_B(n_B-1)}{4} \left(\frac{t}{R} \right)^2. \quad (11)$$

where T_1 corresponds to choosing k out of n_B lines, T_2 refers to the probability that exactly k lines are generated in S , T_3 is the average number of intersections on a single line given that k lines are generated in S , T_4 is due to the fact that including L_0 there are $k+1$ lines in S , and finally, T_5 is to avoid the double counting of the intersections. Similarly, for $t > R$

$$\mathcal{N}_2 = \sum_{k_1=0}^{n_B-1} k_1 \mathcal{P}_\times(t|t > R) = \frac{n_B(n_B-1)}{2\pi R^2} \times \left(t^2 \arcsin \left(\frac{R}{t} \right) + 2R^2 \arccos \left(\frac{R}{t} \right) - R\sqrt{t^2 - R^2} \right). \quad (12)$$

Next, we consider concentric circles centered at the origin having radii $l = \{w, 2w, \dots\}$. In the i -th annulus of width w , the average number of intersections given by (11) and (12) to the area of the annulus gives the intersection density as

$$\rho_{\times, i}(w) = \begin{cases} \frac{1}{\pi w^2 (2i+1)} \left(\frac{n_B(n_B-1)}{4} \times \left(\frac{(w(i+1))^2}{R^2} - \frac{(wi)^2}{R^2} \right) \right); & \text{for } (i+1)w \leq R, \\ \frac{n_B(n_B-1)}{2\pi^2 R^2 w^2 (2i+1)} \left((i+1)^2 w^2 \arcsin \left(\frac{R}{(i+1)w} \right) + 2R^2 \arccos \left(\frac{R}{(i+1)w} \right) - R\sqrt{(i+1)^2 w^2 - R^2} - i^2 w^2 \arcsin \left(\frac{R}{iw} \right) - 2R^2 \arccos \left(\frac{R}{iw} \right) + R\sqrt{i^2 w^2 - R^2} \right); & \text{for } (i+1)w > R. \end{cases}$$

The final result of the intersection radial density can be obtained by substituting $iw = r$ and taking the limit $w \rightarrow 0$.

APPENDIX C PROOF OF THEOREM 3

Proof. Let $f(r)$ be a positive, measurable, monotonic, and bounded function for the first part of the proof. Here, we will find the PGFL of the restricted point process $\Phi' \cap \mathcal{B}((0, 0), t)$. The theorem follows from the monotone convergence theorem with $t \rightarrow \infty$. Note that the distance of a BLP line L_i corresponding to the generating point (r, θ) in \mathcal{D} from $(0, r_0)$ in \mathbb{R}^2 is $l = |r_0 \cos \theta - r|$. A point located at a distance y from the perpendicular projection of $(0, r_0)$ to L_i , has a distance $\sqrt{y^2 + l^2}$ from $(0, r_0)$. The length of the chord is $2\sqrt{t^2 - l^2}$ when $t \geq |r_0 \cos \theta - r|$.

$$G_1(r_0, r, \theta) = \lim_{t \rightarrow \infty} \exp \left(-2\lambda \int_0^{\sqrt{t^2 - l^2}} 1 - f(\sqrt{y^2 + l^2}) dy \right) \stackrel{(a)}{=} \exp \left(-2\lambda \int_0^\infty 1 - f(\sqrt{y^2 + l^2}) dy \right),$$

where step (a) is due to the monotone convergence theorem. In Φ' , each line can either (a) intersect with $\mathcal{B}((0, 0), d_1)$ or (b) does not intersect with $\mathcal{B}((0, 0), d_1)$, where d_1 is the distance from the origin to the nearest point of $\Phi - (0, r_0)$. For a particular r_0 and d_1 , a line is intersecting if $|r_0 \cos \theta - r| \geq d_1$ and non-intersecting otherwise. Thus, we can write the conditional PGFL of the intersecting and non-intersecting lines after averaging over $(r, \theta) \in \mathcal{D}$ as

$$G_1(r_0, d_1) = \frac{1}{A_D(r_0, d_1)} \iint_{\mathcal{D}_B(0, d_1)} \exp \left(-2\lambda \int_{\sqrt{d_1^2 - l^2}}^\infty 1 - f(\sqrt{y^2 + l^2}) dy \right) dr d\theta, \\ G_{NI}(r_0, d_1) = \frac{1}{(2\pi R - A_D(r_0, d_1))} \iint_{\mathcal{D} \setminus \mathcal{D}_B(0, d_1)} \exp \left(-2\lambda \int_0^\infty 1 - f(\sqrt{y^2 + l^2}) dy \right) dr d\theta. \quad (13)$$

Next, note that the line containing the nearest point (at a distance d_1) of the BLCP intersects the disk $\mathcal{B}((0, 0), d_1)$ almost surely. Whereas the other $n_B - 1$ lines may or may not

intersect the disk depending on their generating point. Thus, the PGFL for $\Phi - (0, r_0)$ is evaluated as

$$\begin{aligned}
G(r_0, f(\cdot)) &\stackrel{(a)}{=} \underbrace{G_1(r_0, d_1)}_{T_1} \sum_{n=0}^{n_B-1} \binom{n_B-1}{n} \\
&\quad \left[\underbrace{\left(\frac{A_D(r_0, d_1)}{2\pi R} \times G_1(r_0, d_1) \right)^n}_{T_2} \right. \\
&\quad \left. \times \underbrace{\left(\left(1 - \frac{A_D(r_0, d_1)}{2\pi R} \right) \times G_{NI}(r_0, d_1) \right)^{n_B-n-1}}_{T_3} \right] \\
&\stackrel{(b)}{=} G_1(r_0, d_1) \left(\frac{1}{2\pi R} \right)^{n_B-1} \left(A_D(r_0, d_1) G_1(r_0, d_1) + \right. \\
&\quad \left. (2\pi R - A_D(r_0, d_1)) G_{NI}(r_0, d_1) \right)^{n_B-1}. \quad (14)
\end{aligned}$$

In step (a), the term T_1 corresponds to the line containing the nearest point (recall the Palm perspective discussed in subsection II-E). The term T_2 corresponds to the probability that a set of n lines intersect the disk and the conditional PGFL given that the lines intersect the disk. The term T_3 corresponds to the probability that a set of $n_B - n - 1$ lines do not intersect the disk and the conditional PGFL, given that the lines do not intersect the disk. The statement of the theorem follows from the above. \square

APPENDIX D PROOF OF THEOREM 4

Proof. The success probability can be evaluated as

$$\begin{aligned}
p_S(\gamma) &= \mathbb{P}[\xi(r_0) > \gamma] = \mathbb{P} \left[\frac{\xi_0 d_1^{-\alpha} h_1}{1 + \xi_0 \sum_{\mathbf{x} \in \Phi'} d_{\mathbf{x}}^{-\alpha} h_{\mathbf{x}}} > \gamma \right] \\
&\stackrel{(a)}{=} \mathbb{E} \left[\exp \left(\frac{-\gamma \xi_0 \sum_{\mathbf{x} \in \Phi'} d_{\mathbf{x}}^{-\alpha} h_{\mathbf{x}} - \gamma}{\xi_0 d_1^{-\alpha}} \right) \right] = \mathbb{E}_{d_1} \left[\right. \\
&\quad \left. \exp \left(\frac{-\gamma}{\xi_0 d_1^{-\alpha}} \right) \mathbb{E}_{\mathbf{x}_1, h_{\mathbf{x}}} \left[\exp \left(\frac{-\gamma \sum_{\mathbf{x} \in \Phi'} d_{\mathbf{x}}^{-\alpha} h_{\mathbf{x}}}{d_1^{-\alpha}} \right) \right] \right]. \quad (15)
\end{aligned}$$

In step (a), we use the CCDF of h_1 . Here, $\mathbb{E}_{\mathbf{x}_1}^!$ refers to the expectation taken with respect to the Palm probability of the shifted and reduced point process, i.e., conditioned on the point of $\Phi - (0, r_0)$ being located at \mathbf{x}_1 and then removing it. The 1st term, $\exp \left(\frac{-\gamma}{\xi_0 d_1^{-\alpha}} \right)$, considers noise impact depending solely on d_1 and N_0 , while the second term, $\mathbb{E}_{\mathbf{x}_1, h_{\mathbf{x}}}^! [\cdot]$, addresses interference impact and can be simplified further

$$\begin{aligned}
&\mathbb{E}_{\mathbf{x}_1, h_{\mathbf{x}}}^! \left[\exp \left(\frac{-\gamma \sum_{\mathbf{x} \in \Phi'} d_{\mathbf{x}}^{-\alpha} h_{\mathbf{x}}}{d_1^{-\alpha}} \right) \right] \\
&= \mathbb{E}_{\mathbf{x}_1}^! \left[\prod_{\mathbf{x} \in \Phi'} \left[\mathbb{E}_{h_{\mathbf{x}}} \exp \left(\frac{-\gamma d_{\mathbf{x}}^{-\alpha} h_{\mathbf{x}}}{d_1^{-\alpha}} \right) \right] \right] \\
&= \mathbb{E}_{\mathbf{x}_1}^! \left[\prod_{\mathbf{x} \in \Phi'} \frac{1}{1 + \frac{\gamma d_{\mathbf{x}}^{-\alpha}}{d_1^{-\alpha}}} \right] = G \left(r_0, \frac{1}{1 + \frac{\gamma r^{-\alpha}}{d_1^{-\alpha}}} \right)
\end{aligned}$$

$$\begin{aligned}
&= \frac{1}{A_D(r_0, d_1)} \iint_{\mathcal{D}_B(0, d_1)} \exp \left(-2\lambda \int_{\sqrt{d_1^2 - l^2}}^{\infty} \right. \\
&\quad \left. \left(\frac{\gamma [y^2 + l^2]^{-\frac{\alpha}{2}}}{d_1^{-\alpha} + \gamma [y^2 + l^2]^{-\frac{\alpha}{2}}} \right) dy \right) dr d\theta \times \left(\frac{1}{2\pi R} \right)^{n_B-1} \\
&\quad \left(\iint_{\mathcal{D}_B(0, d_1)} \exp \left(-2\lambda \int_{\sqrt{d_1^2 - l^2}}^{\infty} \left(\frac{\gamma [y^2 + l^2]^{-\frac{\alpha}{2}}}{d_1^{-\alpha} + \gamma [y^2 + l^2]^{-\frac{\alpha}{2}}} \right) dy \right) \right. \\
&\quad \left. dr d\theta + \iint_{\mathcal{D} \setminus \mathcal{D}_B(0, d_1)} \exp \left(-2\lambda \int_0^{\infty} \right. \right. \\
&\quad \left. \left. \left(\frac{\gamma [y^2 + l^2]^{-\frac{\alpha}{2}}}{d_1^{-\alpha} + \gamma [y^2 + l^2]^{-\frac{\alpha}{2}}} \right) dy \right) dr d\theta \right)^{n_B-1}.
\end{aligned}$$

Employing the above in (15) completes the proof. \square